photonics

Communication

High Efficiency and High Bandwidth Double-Cladding Waveguide Photodetector Array for 400 Gbit/s Communication

Fan Xiao [1,2], Han Ye [1], Shuai Wang [1,2], Yimiao Chu [1,2] and Qin Han [1,2,*]

[1] State Key Laboratory on Integrated Optoelectronics, Institute of Semiconductors, Chinese Academy of Sciences, Beijing 100083, China
[2] College of Materials Science and Opto-Electronic Technology, University of Chinese Academy of Sciences, Beijing 100049, China
* Correspondence: hanqin@semi.ac.cn

Abstract: A parallel array of 10 side-illuminated waveguide photodetectors (WGPDs) with double-cladding structure was designed and fabricated. In order to achieve high coupling efficiency to the fiber, the thicknesses of $InGa_{0.24}As_{0.53}P$ cladding layers and $In_{0.53}Ga_{0.47}As$ core layer were optimized. The array exhibited a uniform responsivity of 0.54 A/W at 1310 nm without anti-reflection (AR) coating and dark currents lower than 1.3 nA at −5 V. Each photodetector (PD) showed a bandwidth of over 30 GHz, amounting to 400 Gbit/s transmission capacity for the whole chip. In addition, numerical analysis showed that the fiber alignment tolerance to the chip edge along vertical and horizontal directions, when using a lensed fiber, were 1.8 μm and 4.6 μm, respectively. The simple fabrication, easy alignment capability and high performance make the photodetector array a competitive solution for future 400 Gbit/s parallel communication.

Keywords: photodetector array; double clad; waveguide photodetector; high efficiency

Citation: Xiao, F.; Ye, H.; Wang, S.; Chu, Y.; Han, Q. High Efficiency and High Bandwidth Double-Cladding Waveguide Photodetector Array for 400 Gbit/s Communication. *Photonics* **2022**, *9*, 703. https://doi.org/10.3390/photonics9100703

Received: 13 September 2022
Accepted: 25 September 2022
Published: 28 September 2022

1. Introduction

Driven by the rapid development of big data, cloud computing, and 5G communication networks, the demand for data transmission capacity has grown exponentially [1,2]. In order to meet the heavy traffic in data centers, fiber-based optical interconnections have become a promising scheme, due to their large capacity, high speed, and high reliability [3–5]. At present, the optical communication rate has gradually developed from 25 Gbps/40 Gbps to 100 Gbps/400 Gbps [6]. As the core component of optical receivers, photodetectors play a key role in converting optical signals into electrical signals. High-efficiency, high-sensitivity, and broadband photodetector (PD) arrays are crucial for optical transmission systems [7–9].

Surface-illuminated photodetectors cannot achieve high efficiency in the high frequency region due to the theoretical bandwidth-efficiency limitation [10–12]. To overcome this limitation, side-illuminated waveguide photodetectors (WGPDs) are an attractive alternative [13–15]. Since light and photogenerated carriers are transported in the perpendicular direction, the internal quantum efficiency and bandwidth can be designed almost independently. However, the drawback of conventional InP-$In_{0.53}Ga_{0.47}As$-InP waveguide photodetectors is the poor coupling efficiency with the fiber due to the thin $In_{0.53}Ga_{0.47}As$ layer [16]. Since the $In_{0.53}Ga_{0.47}As$ layer serves as both the carrier transport layer of the PD and the core layer of the waveguide, there is a compromise between coupling efficiency and bandwidth. HO KO et al. [17], in 2018, reported a sport size converter (SSC) integrated waveguide photodetector (WGPD) with a bandwidth of 45 GHz and a responsivity of 0.73 A/W. Sun et al. [18], in 2018, showed an evanescently coupled (EC) WGPD with a bandwidth of 30 GHz and a responsivity of 0.13 A/W and Lin et al. [14], in 2019, investigated an EC WGPD with a bandwidth of 65 GHz and responsivity of 0.19 A/W. These WGPDs are not suitable for PD arrays, due to their complex structures and fabrication processes.

In this paper, we report a parallel array with 10 high-efficiency side-illuminated WGPDs. Each PD contains additional $InGa_{0.24}As_{0.53}P$ cladding layers sandwiching the $In_{0.53}Ga_{0.47}As$ absorber layer. The coupling efficiency of this structure to the fiber is higher than that of the conventional waveguide photodetector, since the vertical optical field distribution is enlarged by the additional $InGa_{0.24}As_{0.53}P$ layer. Meanwhile, the bandwidth is not sacrificed as it is still determined by the thickness of the $In_{0.53}Ga_{0.47}As$ layer. The measurement results showed that the 10 WGPDs exhibited uniform responsivities over 0.54 A/W at 1310 nm without anti-reflection (AR) coating on the edge facet and low dark currents of about 1.3 nA at 5 V reverse bias. The PD array has the total transmission speed exceeds 400 Gbit/s, and it provides a low-cost solution for both monolithic integration and heterogeneous integration platforms (PLC, SiP, etc) [19,20].

2. Design and Simulation

The PD array includes 10 waveguide PIN photodetectors with a spacing of 750 μm, which is compatible with the commercially available trans-impedance amplifier electrode spacing, and the three-dimensional (3D) schematic structure of a single PD is shown in Figure 1. To achieve great coupling to a fiber in the y direction, each PD has a 5 μm wide high-mesa structure. The photodetector epitaxial structure is symmetrical, which includes a semi-insulating InP substrate, a 0.5 μm thick n^+-doped (Si: 5×10^{18} cm^{-3}) InP cladding layer, an n-doped (Si: 1×10^{18} cm^{-3}) InGaAsP cladding layer, an intrinsic $In_{0.53}Ga_{0.47}As$ absorption layer, a p-doped (Zn: 1×10^{18} cm^{-3}) InGaAsP cladding layer, a 0.5 μm thick p^+-doped (Zn: 3×10^{18} cm^{-3}) InP cladding layer and a 0.08 μm thick p^+-doped (Zn: 1×10^{19} cm^{-3}) $In_{0.53}Ga_{0.47}As$ ohmic contact layer. The $In_{0.53}Ga_{0.47}As$ absorption layer is sandwiched between n-InP/InGaAsP and p-InGaAsP/InP cladding layers. To obtain wide vertical optical field distribution in the WGPD, and make the InGaAsP cladding layers transparent to the input light at 1310 nm, we defined the InGaAsP as $InGa_{0.24}As_{0.53}P$ (λ_g = 1.24 μm).

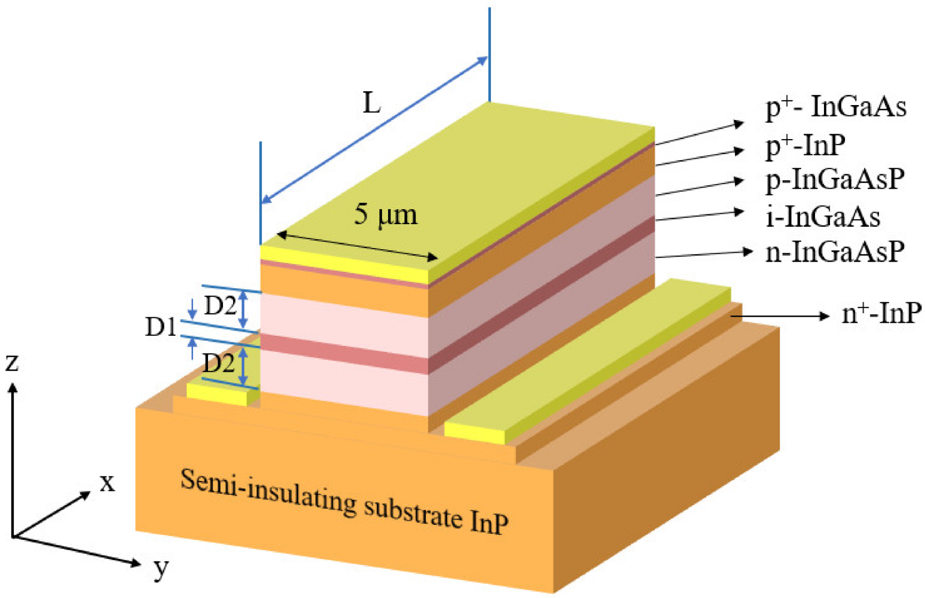

Figure 1. The three-dimensional schematic structure of the single photodetector (PD).

The quantum efficiency η in the WGPD can be described by the following equation [21]:

$$\eta = (1 - R) \times \left(1 - e^{-\alpha\Gamma L}\right) \times \eta_C \tag{1}$$

where R is power reflection loss on the facet of the WGPD, α is the absorption coefficient of $In_{0.53}Ga_{0.47}As$ at 1310 nm, Γ is the optical confinement factor of the $In_{0.53}Ga_{0.47}As$ layer, L is the WGPD length and η_C is the coupling efficiency to fiber. In this structure, with a constant InP cladding thickness of 0.5 μm, the Γ and η_C in the WGPD is simultaneously determined by the $In_{0.53}Ga_{0.47}As$ layer and the $InGa_{0.24}As_{0.53}P$ layer. In order to improve responsivity with a large 3 dB bandwidth, the $In_{0.53}Ga_{0.47}As$ layer thickness D1, the $InGa_{0.24}As_{0.53}P$ layer thickness D2 and the WGPD length L were investigated. Large photo-absorption characteristics and a large mode field in the waveguide structure should be obtained in order to achieve high responsivity.

The optical transmission of the structure was simulated by three-dimensional finite-difference time-domain (3D FDTD) methods. The simulated cross-section optical power distributions of the WGPD with different $InGa_{0.24}As_{0.53}P$ layer thicknesses D2 are depicted in Figure 2. The mode field in the WGPD clearly expanded in the z-axis direction by introducing the $InGa_{0.24}As_{0.53}P$ layer, which could effectively reduce the coupling loss caused by the mode field mismatch between the WGPD and the fiber. Figure 3a exhibits the simulated quantum efficiency versus $InGa_{0.24}As_{0.53}P$ thickness D2 under different $In_{0.53}Ga_{0.47}As$ thicknesses D1. For a fixed value of D1, the quantum efficiency did not vary monotonically with D2, which was attributed to the inverse relationship between the coupling efficiency η_C and the optical confinement factor Γ as the $InGa_{0.24}As_{0.53}P$ thickness D2 changed. Nevertheless, it could also be observed from Figure 3a that the quantum efficiency with nonzero $InGa_{0.24}As_{0.53}P$ layer thickness D2 was significantly higher than that of D2 = 0; particularly, when D1 = 0.2 μm and D2 = 0.9 μm, when the quantum efficiency doubled. Therefore, for the same D1, the quantum efficiency could be specified relatively independent of the bandwidth.

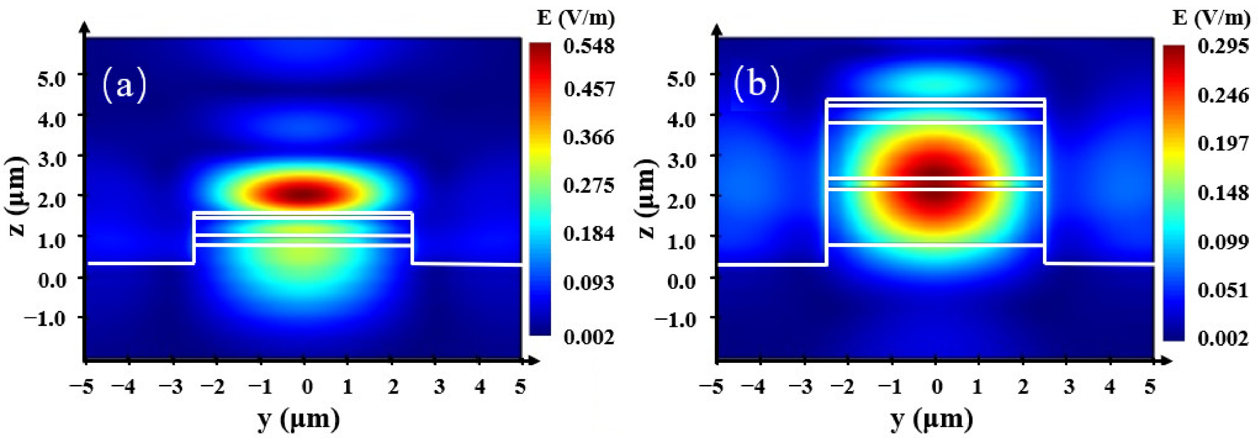

Figure 2. Cross-section of the waveguide photodetector (WGPD) with different $InGa_{0.24}As_{0.53}P$ layer thicknesses: (**a**) 0 μm thick $InGa_{0.24}As_{0.53}P$ layer and 0.2 μm thick $In_{0.53}Ga_{0.47}As$ layer. (**b**) 1.4 μm thick $InGa_{0.24}As_{0.53}P$ layer and 0.2 μm thick $In_{0.53}Ga_{0.47}As$ layer.

In addition, the simulated optical power transmission of the absorption region is shown in Figure 3b. Since the light is injected directly into the edge of the absorber layer, the input light is mostly absorbed at the front end of the PD. At a fixed $In_{0.53}Ga_{0.47}As$ thickness D1 = 0.2 μm. The WGPD length L dependent quantum efficiency for the values of $InGa_{0.24}As_{0.53}P$ thickness D2 = 0.85 and 1 μm is also presented in Figure 3c, from which it can be seen that the quantum efficiency was almost stable when the detector length exceeded 20 μm. In this case, in order to reduce the photodetector series resistance and diode capacitance, the optimized parameters of the WGPD were chosen to be D1 = 0.2 μm, D2 = 0.85 μm and L = 20 μm for further simulations and experiments.

Fiber misalignment tolerance to WGPD with optimized parameters is also plotted in Figure 3d. At −1 dB power reduction, the alignment tolerances of the chip along the vertical and horizontal directions were 1.8 μm and 4.6 μm, respectively. Therefore, the double-clad WGPD could be easily coupled with the fiber.

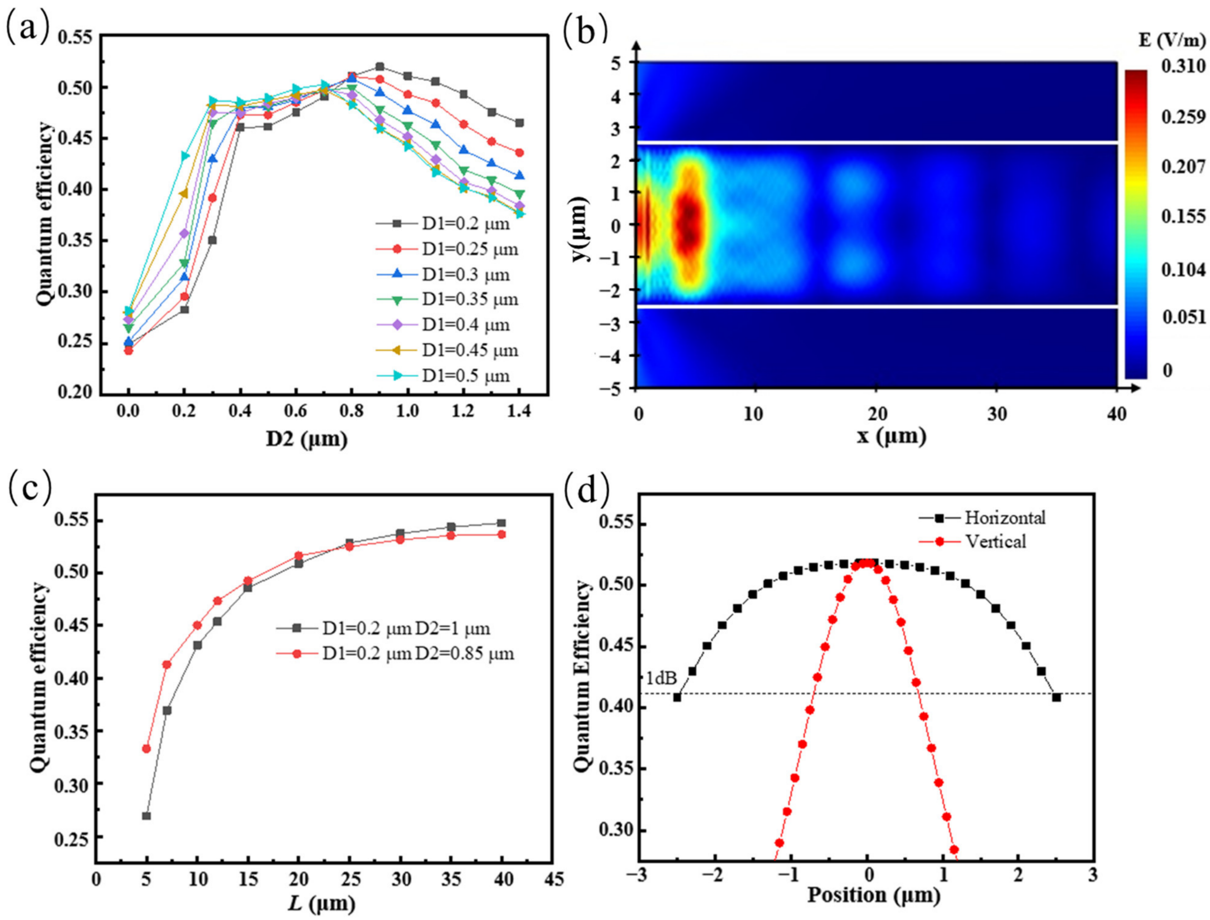

Figure 3. (**a**) Plots of simulated quantum efficiency versus $InGa_{0.24}As_{0.53}P$ layer thickness D2 under different value of $In_{0.53}Ga_{0.47}As$ layer thickness D1. (**b**) Simulated optical power transmission in the absorption region with a 0.2 μm $In_{0.53}Ga_{0.47}As$ absorption layer and a 0.85 μm $InGa_{0.24}As_{0.53}P$ cladding layer. (**c**) Simulated quantum efficiency dependence on waveguide length. (**d**) Dependence of quantum efficiency upon the position of lensed Single Mode Fiber (SMF). 1 dB alignment tolerance is 1.8 μm and 4.6 μm in vertical and horizontal direction, respectively.

3. Chip Fabrication

The epitaxial structure was grown by the metal-organic chemical vapor deposition (MOCVD) technique on a semi-insulating InP substrate. PD array mesas were fabricated by contact ultraviolet lithography technology and inductively coupled plasma (ICP)etching. The SiO_2 passivation film was deposited by plasma enhanced vapor deposition (PECVD). Then polyimide was spun for planarization and patterned for metal contacts. After that, N electrodes and coplanar microwave lines were deposited by magnetron sputtering of AuGeNi/Au and Ti/Au, respectively. Finally, the fabricated PD array was precisely cleaved to a 20 μm length by an automated cleavage machine.

4. Measurements and Result Analysis

The dark current measurements of the PD array were performed by the KEITHLEY 4200 Semiconductor Tester at room temperature. Figure 4 shows the I–V characteristic curves of these photodiodes at a bias voltage from −5 to 1 V. The dark currents of these photodiodes with an active region of $5 \times 20\ \mu m^2$ were in the range of 0.6–1.3 nA at 5 V reverse bias, which benefited from effective mesa passivation and small etching damages. These low dark current values were critical for the high sensitivity of the PD array.

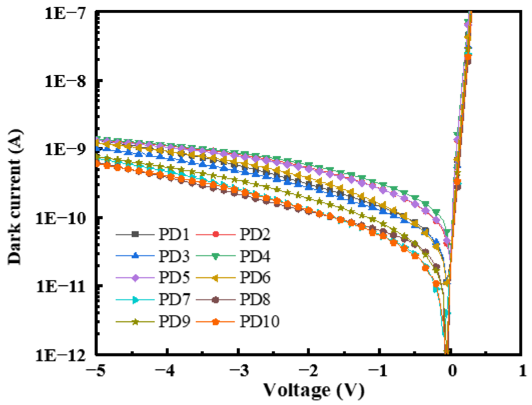

Figure 4. The dark current measurement result of the photodetector array.

Photo-response measurements were carried out using a 1310 nm laser source, a tapered fiber with a 2.5 μm spot size and a KEITHLEY 4200 Semiconductor Tester. The fiber output power and the bias voltage were fixed at 1.02 mW and −5 V, respectively. The results of measured photocurrent and calculated responsivity are shown in Figures 5a and 5b, respectively. All 10 WGPDs exhibited a uniform responsivity over 0.54 A/W without an AR coating. The quantum efficiency of the single PD was deduced to be 51%, which was consistent with the simulated value. By depositing an AR coating on the input facet, the quantum efficiency was expected to exceed 72% as the reflection loss would be negligible. Therefore, the double-cladding scheme could achieve high quantum efficiency without introducing a spot size converter in WGPD, which facilitated compact and large-scale on-chip integration.

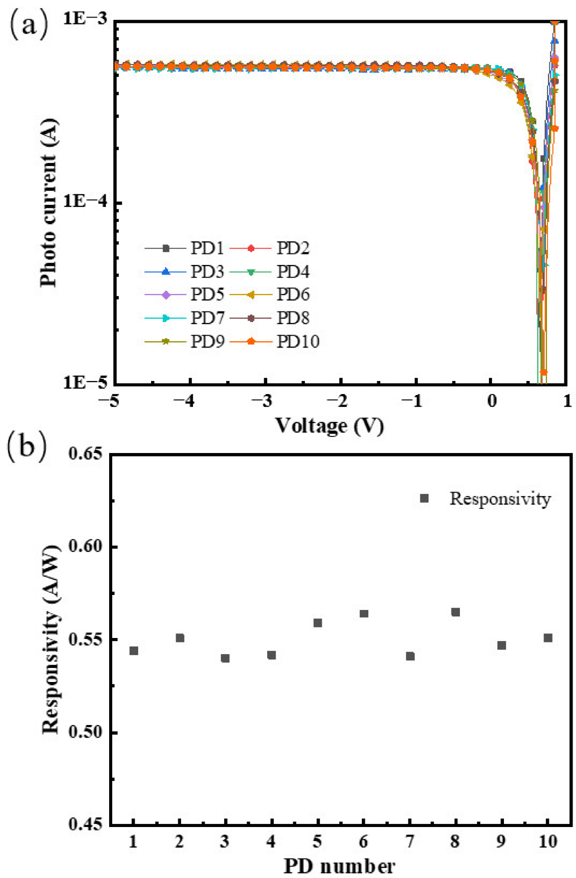

Figure 5. (**a**) The photocurrent measurement result of the photodetector array as a function of voltage bias without an anti-reflection (AR) coating, (**b**) The responsivity result of the photodetector array without an anti-reflection (AR) coating.

The frequency response measurement setup was based on a Vector network analyzer in the test range from 10 MHz to 40 GHz. Figure 6 shows the measurement result at −5 V bias. All 10 units of the PD array exhibited a uniform −3 dB bandwidth over 30 GHz, and the whole chip was suitable for 400 Gbit/s data transmission system. The typical bandwidth calculation formula [22] is as follows:

$$\frac{1}{f_{3dB}^2} \cong \frac{1}{f_t^2} + \frac{1}{f_{RC}^2} \tag{2}$$

$$f_t \cong \frac{3.5\,\overline{v}}{2\pi D} \tag{3}$$

$$f_{RC} \cong \frac{1}{2\pi(C_P + C_j)(R_L + R_S)} \tag{4}$$

where f_t and f_{RC} are the carrier transit-time limited bandwidth and the resistance–capacitance (RC) time constant limited bandwidth. $\overline{v}$ is the average velocity of electron and hole. D is the intrinsic layer thickness. C_P and C_j are the parasitic capacitance and diode capacitance. R_L and R_s are the load resistance and series resistance, respectively. The calculated f_t was about 147.6 GHz and f_{RC} was 34.3 GHz, thus, the calculated f_{3dB} was about 33.5 GHz. Obviously, the main factor that limited the device's bandwidth came from the series resistance and the diode capacitance, which greatly reduced the RC bandwidth. Bandwidth of photodetectors could be further improved by optimizing alloy conditions, to decrease the series resistance, and shrinking device size, to reduce diode capacitance.

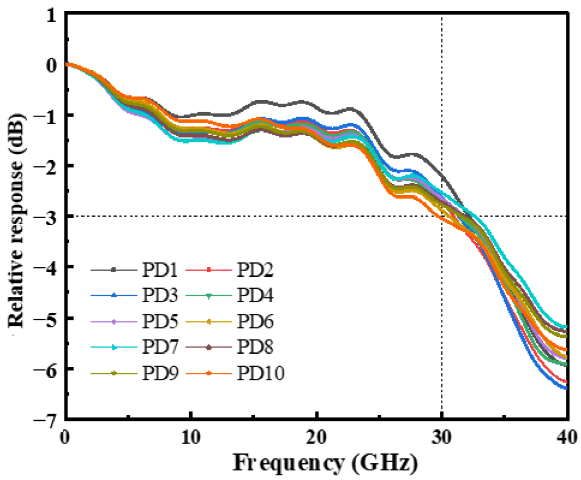

Figure 6. Frequency response measurement result of the photodetector (PD) array at 5 V reverse bias.

5. Conclusions

We designed and fabricated a PD array containing a 10 double-cladding waveguide structure. The PD array overcame the limitation of coupling efficiency and bandwidth in conventional WGPDs, and was easy to fabricate. The 0.2 µm $In_{0.53}Ga_{0.47}As$ absorber thickness, 0.85 µm $InGa_{0.24}As_{0.53}P$ cladding thickness, and 20 µm photodetector length were optimized to achieve a high quantum efficiency of 52%, twice that of the conventional InP-$In_{0.53}Ga_{0.47}As$-InP WGPD. The 10 PDs all exhibited good responsivity of 0.54 A/W at 1310 nm, uniform low dark current of 1.3 nA at 5 V reverse bias, and 3 dB bandwidth beyond 30 GHz, in good agreement with the theoretical expectations. The high-frequency characteristics of PD arrays would be greatly improved by optimizing alloy conditions and reducing device size. Moreover, the simulated alignment tolerance to the chip along vertical and horizontal direction was 1.8 µm and 4.6 µm, respectively. These results demonstrate that the PD array has application advantages as a low-cost, high-efficiency, high-speed, and high-sensitivity parallel communication system.

Author Contributions: Formal analysis, F.X. and Q.H.; funding acquisition, Q.H. and H.Y.; software, F.X.; experiments and tests, F.X.; writing—original draft, F.X.; writing—editing, Q.H., H.Y., S.W. and Y.C. All authors have read and agreed to the published version of the manuscript.

Funding: This research was funded by the National Key Research and Development program of China (No. 2020YFB1805701), the National Natural Science Foundation of China (Nos. 61934003, 61635010, 61674136).

Institutional Review Board Statement: Not applicable.

Informed Consent Statement: Not applicable.

Data Availability Statement: The data that support the findings of this study are available from the corresponding author upon reasonable request.

Conflicts of Interest: The authors declare no conflict of interest.

References

1. Zhou, X.; Liu, H.; Urata, R.; Zebian, S. Scaling large data center interconnects: Challenges and solutions. *Opt. Fiber Technol.* **2018**, *44*, 61–68. [CrossRef]
2. Miguelez, P. What Applications are Driving Higher Capacity in Access? In Proceedings of the 2018 Optical Fiber Communications Conference and Exposition (ofc), San Diego, CA, USA, 11–15 March 2018; IEEE: New York, NY, USA, 2018.
3. Runge, P.; Beckerwerth, T.; Troppenz, U.; Gruner, M.; Boerma, H.; Mohrle, M.; Schell, M. InP-Components for 100 GBaud Optical Data Center Communication. *Photonics* **2021**, *8*, 18. [CrossRef]
4. Johari, A.; Bhatnagar, A.; Naithani, S.; Kaushik, B.K. Performance analysis of Vertical Photodetector for Efficient on Chip Optical Interconnect. In Proceedings of the Novel Optical Systems, Methods, and Applications XXIII, online, 24 August–4 September 2020; Hahlweg, C.F., Mulley, J.R., Eds.; Spie-Int Soc Optical Engineering: Bellingham, MA, USA, 2020; Volume 11483, p. 114830L.
5. Lam, C.F.; Liu, H.; Koley, B.; Zhao, X.; Kamalov, V.; Gill, V. Fiber Optic Communication Technologies: What's Needed for Datacenter Network Operations. *IEEE Commun. Mag.* **2010**, *48*, 32–39. [CrossRef]
6. Kachris, C.; Kanonakis, K.; Tomkos, I. Optical Interconnection Networks in Data Centers: Recent Trends and Future Challenges. *IEEE Commun. Mag.* **2013**, *51*, 39–45. [CrossRef]
7. Bottacchi, S.; Beling, A.; Matiss, A.; Nielsen, M.L.; Steffan, A.G.; Unterboersch, G.; Umbach, A. Advanced Photoreceivers for High-Speed Optical Fiber Transmission Systems. *IEEE J. Sel. Top. Quantum Electron.* **2010**, *16*, 1099–1112. [CrossRef]
8. Nada, M.; Nakajima, F.; Yoshimatsu, T.; Nakanishi, Y.; Kanda, A.; Shindo, T.; Tatsumi, S.; Matsuzaki, H.; Sano, K. Inverted p-down Design for High-Speed Photodetectors. *Photonics* **2021**, *8*, 39. [CrossRef]
9. Xu, J.; Zhang, X.; Kishk, A. Design of high speed InGaAs/InP one-sided junction photodiodes with low junction capacitance. *Opt. Commun.* **2019**, *437*, 321–329. [CrossRef]
10. Achouche, M.; Glastre, G.; Caillaud, C.; Lahrichi, M.; Chtioui, M.; Carpentier, D. InGaAs Communication Photodiodes: From Low-to High-Power-Level Designs. *IEEE Photonics J.* **2010**, *2*, 460–468. [CrossRef]
11. Li, C.; Xue, C.; Liu, Z.; Cheng, B.; Li, C.; Wang, Q. High-Bandwidth and High-Responsivity Top-Illuminated Germanium Photodiodes for Optical Interconnection. *IEEE Trans. Electron. Devices* **2013**, *60*, 1183–1187. [CrossRef]
12. Ito, H.; Kodama, S.; Muramoto, Y.; Furuta, T.; Nagatsuma, T.; Ishibashi, T. High-speed and high-output InP-InGaAs unitraveling-carrier photodiodes. *IEEE J. Sel. Top. Quantum Electron.* **2004**, *10*, 709–727. [CrossRef]
13. Yin, T.; Cohen, R.; Morse, M.M.; Sarid, G.; Chetrit, Y.; Rubin, D.; Paniccia, M.J. 31 GHz Ge n-i-p waveguide photodetectors on Silicon-on-Insulator substrate. *Opt. Express* **2007**, *15*, 13965–13971. [CrossRef]
14. Lin, X.; Natrella, M.; Seddon, J.; Graham, C.; Renaud, C.C.; Tang, M.; Wu, J.; Liu, H.; Seeds, A.J. High performance waveguide uni-travelling carrier photodiode grown by solid source molecular beam epitaxy. *Opt. Express* **2019**, *27*, 37065–37086. [CrossRef] [PubMed]
15. Sun, K.; Gao, J.; Jung, D.; Bowers, J.; Beling, A. 40 Gbit/s waveguide photodiode using III-V on silicon heteroepitaxy. *Opt. Lett.* **2020**, *45*, 2954–2956. [CrossRef]
16. Shao-Qing, L.; Xiao-Hong, Y.; Yu, L.; Bin, L.; Qin, H. Design and fabrication of a high-performance evanescently coupled waveguide photodetector. *Chin. Phys. B* **2013**, *22*, 108503. [CrossRef]
17. Ko, Y.-H.; Choe, J.-S.; Han, W.S.; Lee, S.-Y.; Han, Y.-T.; Jung, H.-D.; Youn, C.J.; Kim, J.-H.; Baek, Y. High-speed waveguide photodetector for 64 Gbaud coherent receiver. *Opt. Lett.* **2018**, *43*, 579–582. [CrossRef] [PubMed]
18. Sun, S.; Liang, S.; Xie, X.; Xu, J.; Guo, L.; Zhu, H.; Wang, W. Zero-bias 32 Gb/s evanescently coupled InGaAs/InP UTC-PDs. *Opt. Laser Technol.* **2018**, *101*, 457–461. [CrossRef]
19. Li, S.; Wang, L.; An, J.; Zhang, J.; Huang, N.; He, W.; Wang, Y.; Yin, X.; Wang, H.; Li, J.; et al. Eight-wavelength receiver optical subassembly based on silica hybrid integrated technology. *Opt. Eng.* **2019**, *58*, 097101. [CrossRef]

20. Okimoto, T.; Yagi, H.; Ebihara, K.; Yamazaki, K.; Okamoto, S.; Ohkura, Y.; Horino, K.; Ashizawa, K.; Ekawa, M.; Yoneda, Y. InP-based PIC integrated with Butt-joint Coupled Waveguide p-i-n PDs for 100GBaud Coherent Networks. In Proceedings of the 2021 Optical Fiber Communications Conference and Exposition (OFC), San Francisco, CA, USA, 6–10 June 2021; IEEE: New York, NY, USA, 2021; p. F2C.6.
21. Kato, K.; Hata, S.; Kozen, A.; Oku, S.; Matsumoto, S.; Yoshida, J. 22 Ghz Photodiode Monolithically Integrated with Optical Wave-Guide on Semiinsulating Inp Using Novel Butt-Joint Structure. *Electron. Lett.* **1992**, *28*, 1140–1142. [CrossRef]
22. Achouche, M.; Magnin, V.; Harari, J.; Carpentier, D.; Derouin, E.; Jany, C.; Decoster, D. Design and fabrication of a p-i-n photodiode with high responsivity and large alignment tolerances for 40-Gb/s applications. *IEEE Photonics Technol. Lett.* **2006**, *18*, 556–558. [CrossRef]